



Nanoscale organization by elastic interactions between H and He platelets in Si

Shay Reboh, J-F. Barbot, Maxime Vallet, M.F. Beaufort, F. Rieutord, F.
Mazen, Nikolay Cherkashin, P.F.P. Fichtner, J. Grilhé

► To cite this version:

Shay Reboh, J-F. Barbot, Maxime Vallet, M.F. Beaufort, F. Rieutord, et al.. Nanoscale organization by elastic interactions between H and He platelets in Si. *Journal of Applied Physics*, 2013, 114 (7), pp.073517. 10.1063/1.4818812 . hal-01736021

HAL Id: hal-01736021

<https://hal.science/hal-01736021>

Submitted on 22 Mar 2018

HAL is a multi-disciplinary open access archive for the deposit and dissemination of scientific research documents, whether they are published or not. The documents may come from teaching and research institutions in France or abroad, or from public or private research centers.

L'archive ouverte pluridisciplinaire **HAL**, est destinée au dépôt et à la diffusion de documents scientifiques de niveau recherche, publiés ou non, émanant des établissements d'enseignement et de recherche français ou étrangers, des laboratoires publics ou privés.

Nanoscale organization by elastic interactions between H and He platelets in Si

S. Reboh, J. F. Barbot, M. Vallet, M. F. Beaufort, F. Rieutord, F. Mazen, N. Cherkashin, P. F. P. Fichtner, and J. Grilhé

Citation: *Journal of Applied Physics* **114**, 073517 (2013); doi: 10.1063/1.4818812

View online: <https://doi.org/10.1063/1.4818812>

View Table of Contents: <http://aip.scitation.org/toc/jap/114/7>

Published by the American Institute of Physics

Articles you may be interested in

[Effect of the substrate orientation on the formation of He-plates in Si](#)

Journal of Applied Physics **114**, 193501 (2013); 10.1063/1.4831659

[In situ growth and coalescence of He-filled bi-dimensional defects in Si by H supply](#)

Journal of Applied Physics **115**, 223515 (2014); 10.1063/1.4883766

[In-situ evolution of helium bubbles in SiC under irradiation](#)

Journal of Applied Physics **118**, 205904 (2015); 10.1063/1.4936562

[Cracks and blisters formed close to a silicon wafer surface by He-H co-implantation at low energy](#)

Journal of Applied Physics **118**, 245301 (2015); 10.1063/1.4938108

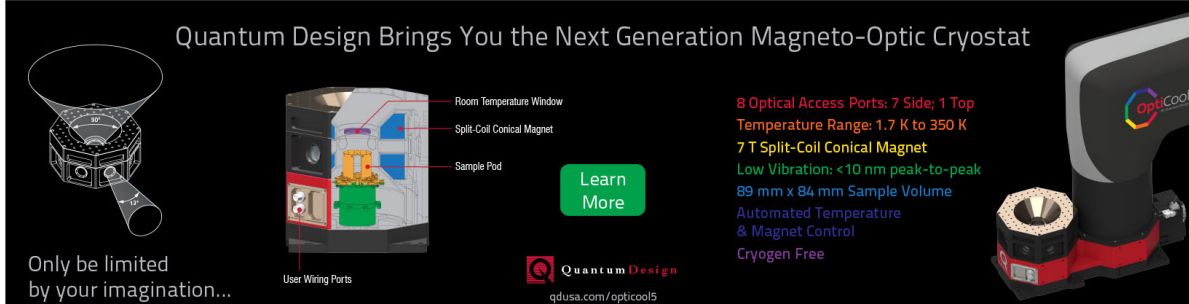
[Lithium implantation at low temperature in silicon for sharp buried amorphous layer formation and defect engineering](#)

Journal of Applied Physics **113**, 083515 (2013); 10.1063/1.4793507

[Effect of the order of He⁺ and H⁺ ion co-implantation on damage generation and thermal evolution of complexes, platelets, and blisters in silicon](#)

Journal of Applied Physics **119**, 135308 (2016); 10.1063/1.4945032

Quantum Design Brings You the Next Generation Magneto-Optic Cryostat



Only be limited by your imagination...

Room Temperature Window
Split-Coil Conical Magnet
Sample Pod
User Wiring Ports

Learn More

Quantum Design
qdusa.com/opticool5

8 Optical Access Ports: 7 Side; 1 Top
Temperature Range: 1.7 K to 350 K
7 T Split-Coil Conical Magnet
Low Vibration: <10 nm peak-to-peak
89 mm x 84 mm Sample Volume
Automated Temperature & Magnet Control
Cryogen Free

OptiCool

Nanoscale organization by elastic interactions between H and He platelets in Si

S. Reboh,^{1,a)} J. F. Barbot,² M. Vallet,² M. F. Beaufort,² F. Rieutord,³ F. Mazen,¹
 N. Cherkashin,⁴ P. F. P. Fichtner,⁵ and J. Grilhé²

¹CEA-LETI, Minatec Campus, 17 rue des Martyrs, 38054 Grenoble, France

²Institut Prime (UPR 3346), Department of Material Sciences, CNRS, Université de Poitiers, ENSMA, BP30179, 86962 Futuroscope Chasseneuil, France

³CEA-Grenoble, INAC-SP2M, 38054 Grenoble, France

⁴CEMES, CNRS UPR 8011 and Université de Toulouse, 29 rue Jeanne Marvig, 31055 Toulouse, France

⁵Escola de Engenharia, Universidade Federal do Rio Grande do Sul, Porto Alegre 91501-970, Brazil

(Received 15 May 2013; accepted 2 August 2013; published online 21 August 2013)

We used ion implantation of H and He in Si and thermal treatments to produce two systems allowing to study the effects of global and local mechanical stress fields on the formation energy of H-precipitates called H-platelets. In the first part of the work, the depth-distribution of different crystallographic orientations of the precipitates formed along the implanted layer was characterized by transmission electron microscopy. The global strain in the region was measured by X-ray diffraction, and the depth distribution of strain was reconstructed using a dynamical-theory-based code. Elasticity theory was used to develop a model based on mechanical interactions, explaining the preferential presence of (001)-oriented precipitates in the more stressed region of the implanted layer. In a second part, local sources of stress of nanometer size and cylindrical symmetry were introduced in a deeper region of the matrix, before the nucleation of H-platelets. The local stresses were embodied by (001) He-plate precipitates. Upon annealing, a specific arrangement of crystallographic variants of {111}-oriented H-platelets in a four-fold configuration was observed. To explain these experimental observations, and to calculate the variations of the formation energy of the precipitates under the presence of local stress tensors components, analytical and numerical (finite element method) approaches were used to develop 2D and 3D models based on elasticity theory. The concepts and modeling strategy developed here paves the way for determining the required conditions to create controlled architecture of precipitates at the nanoscale using local stress engineering. © 2013 AIP Publishing LLC. [<http://dx.doi.org/10.1063/1.4818812>]

I. INTRODUCTION

The spatial organization of nano-objects is a challenge that requires the development of disruptive concepts. There are essentially two different approaches to manipulate and arrange nano-objects at the nanoscale: (i) top-down approach, based on a direct interference in the system, for example, by producing lithographic patterns to mediate organization, and (ii) bottom-up approach, from which organization emerges from the physical interactions in the system, producing what has been referred to as self-assembly. Top-down concepts are dominant for industrial applications; however, bottom-up processes are regarded as important and sophisticated concepts to be developed for future nanofabrication. Therefore, there is a fundamental and technological interest in innovative approaches and on understanding organization at the nanoscale.^{1,2}

In this context, we have demonstrated that the interaction between nanoscopic stress fields can be used to select crystallographic variants of precipitates in spatially defined regions, and then, to create innovative arrangements embedded in a crystalline matrix.³ Here, we present an extensive and detailed structural characterization and modeling of this system. Our experiment consists in using ion implantation

and thermal annealing processes to produce a planar arrangement of bi-dimensional plate-like precipitates filled with helium gas.⁴⁻⁷ These objects, of typical diameter at the order of 100 nm, generate local stress fields of cylindrical symmetry at the nanoscale range. Under the influence of such stresses, we induced the formation of smaller (typically of 10 to 20 nm diameter) bi-dimensional plate-like precipitates of hydrogen. The cylindrical nature of the stress field emerging from the He-plates patterned the precipitation of H-platelets in a four-fold configuration. The effect of elastic interactions on the formation energy of different crystallographic variants of H-platelets is modeled in 2D using analytical approaches, and in 3D using numerical calculations. The predictions of the model and extensions of the concept as a method to organize precipitates at the nanoscale dimension are discussed.

II. EXPERIMENTAL

The substrates used in this study were 1–25 Ω cm p-type (001) Czochralski grown Si crystals of 750 μ m thickness.

Experiment I: The first experiment was intended to evaluate the impact of the in-plane biaxial stress generated by the lattice damage introduced by the implantation process on the nucleation and precipitation of H-platelets.¹¹ For this, a Si substrate was implanted with H_2^+ ions to the fluence of $0.5 \times 10^{16} \text{ cm}^{-2}$ and incident energy of 30 keV. According to

^{a)}Author to whom correspondence should be addressed. Electronic mail: shay.reboh@cea.fr

SRIM calculations,¹² the projected ion range R_p is of ≈ 200 nm from the surface. After implantation, the lattice strain $(\Delta d/d)_z$ associated to the implanted layer,^{8–10} appearing along the direction normal to the surface and referred to as out-of-plane strain, was measured by X-ray diffraction (XRD) scans around the (004) reflection of the Si substrate. The experiments were performed using a Philips X'Pert equipment. Another piece was annealed at 300 °C for 1800 s to induce the precipitation of H-platelets. The microstructure of the annealed material was characterized by Transmission Electron Microscopy (TEM).

Experiment II: The second experiment was carried out to study the influence of a nanoscale stress-field on the precipitation of H. The samples were prepared in two-steps of implantation/annealing. In step one, the Si substrate was implanted with 45 keV He⁺ ions to the fluence of $1 \times 10^{16} \text{ cm}^{-2}$ and annealed at 350 °C for 900 s. Pressurized He-plates^{4–6} oriented parallel to the surface are expected to form at a depth close to the projected range of the ions ($R_p^{\text{He}} \approx 385$ nm), producing a 2D array of nanoscale stress-field sources. In the second step, 30 keV H₂⁺ ions at the fluence of $0.5 \times 10^{16} \text{ cm}^{-2}$ were implanted, and the substrate was annealed at 300 °C for 1800 s to form the H-platelets. As in experiment I, the precipitation of H-platelets is intended to take place at ≈ 200 nm depth, at half distance from the He-plates to the substrate surface. After each step of preparation, samples were characterized by TEM.

All the implantations were performed at room temperature using a beam current density of $\approx 0.5 \mu\text{A cm}^{-2}$, and thermal treatments were done under high vacuum in a quartz tube and a resistance furnace. The TEM investigations in cross-section and plan-view were performed in a JEM 2010 Microscope operating at 200 kV. The specimens were prepared by mechanical polishing and ion milling.

III. RESULTS AND DISCUSSIONS

A. The effect of in-plane stress on the nucleation of H-platelets (experiment I)

Figure 1(a) displays the XRD diffraction pattern obtained after H-implantation in as-implanted condition. The curve exhibits a principal sharp peak at the angle $\theta_B = 34.57^\circ$ referent to the (004) Bragg reflection of the pristine Si substrate. For $\theta < \theta_B$, additional intensities are observed. The pattern is characteristic of a lattice dilatation gradient of Gaussian-like shape along the normal to the surface (z-direction defined as [001] direction).^{8–10} The XRD diffraction pattern was simulated using the web-based code GID_SL written by Stepanov.¹³ The simulation of the curve (displayed as dotted line in Fig. 1(a)), allowed the reconstruction of the strain depth-profile shown in the inset in Fig. 1(a), presenting a maximum strain $\varepsilon_{zz}^{\text{MAX}} \approx 0.35\%$. Figure 1(b) shows a cross-sectional TEM image of the material after annealing at 300 °C for 1800 s. H-platelets parallel to the surface are predominantly seen in the central region of the implanted layer and platelets of {111}-orientations are more frequent at the upper and lower borders.

To develop an analytical model to describe the influence of the external stress field introduced by the implantation on

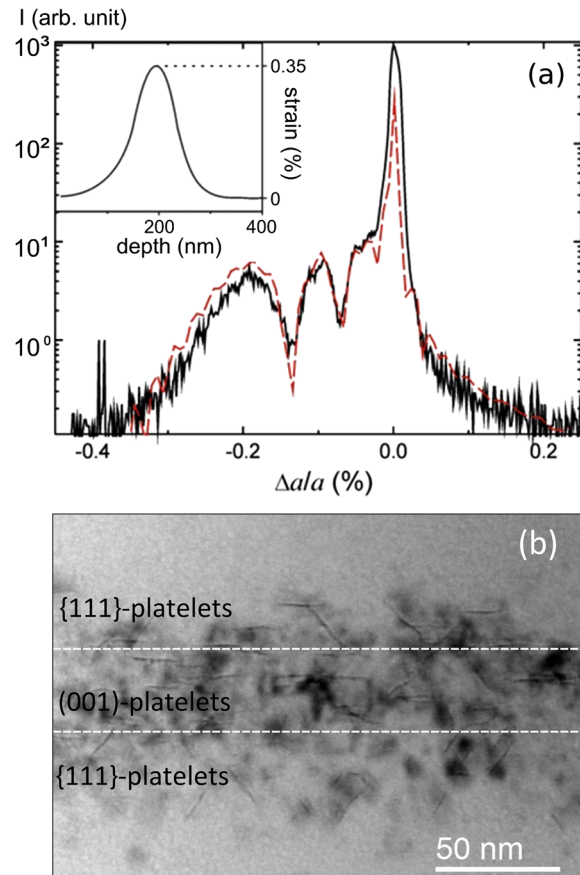


FIG. 1. (a) x-ray diffraction measurement showing the scattered intensity around the (004) reflection of the Si substrate, obtained from the as-implanted sample (30 keV H₂⁺ at the fluence of $0.5 \times 10^{16} \text{ cm}^{-2}$). The simulated curve (dotted line) is superimposed to the experimental data, and the reconstructed depth-distribution of strain is displayed in the inset. (b) Cross-sectional TEM micrograph of a Si substrate implanted with 30 keV H₂⁺ at the fluence of $0.5 \times 10^{16} \text{ cm}^{-2}$ and annealing at 300 °C for 1800 s. It highlights the repartition of crystallographic variants of H-platelets observed along depth z.

the formation energy of H-platelets, and consequently on the preferential appearance of certain crystallographic variants, first, we have to describe the stress tensor. The origin of strain/stress in H-implanted Si is related to the introduction of foreign atoms and lattice disorder in the material.^{8,10,14–16} These structural modifications cause a localized increase of volume within the damaged layer, or an isotropic intrinsic strain e .^{14–16} Along the z-direction perpendicular to the surface, there is no restriction to deformation and the system can assume its new configuration. In the directions parallel to the surface (defined here as x and y), however, the thick substrate imposes a restriction to relaxation. Therefore, there is an elastic compressive in-plane strain which develops to oppose e . This effect generates an in-plane stress and, by Poisson reaction, elastic strains appear along z. We can write then that the total out-of-plane strain $\varepsilon_{zz}^{\text{tot}}$ measured by XRD is composed of elastic and intrinsic contributions¹⁶ as

$$\begin{aligned} \varepsilon_{zz}^{\text{tot}} &= \varepsilon_{zz}^* + e, \\ \varepsilon_{yy}^* &= \varepsilon_{xx}^* = -e, \end{aligned} \quad (1)$$

where the superscript * stands for the elastic strains.

Assuming a plane-stress configuration, where the stress components dependent on z are null and the in-plane stress $\sigma_{//} = \sigma_{yy} = \sigma_{xx}$, the relations in Eq. (1) can be combined with the generalized Hooke's law to write that

$$\sigma_{//} = -2\mu\epsilon_{zz}^{tot}(z), \quad (2)$$

where μ is the shear modulus of the material and $\epsilon_{zz}^{tot}(z)$ follows a Gaussian-like distribution as

$$\epsilon_{zz}^{tot}(z) = \epsilon_{zz}^{MAX} e^{\left(-\frac{(z-Rp)^2}{2(\Delta Rp)^2}\right)}, \quad (3)$$

where ϵ_{zz}^{MAX} stands for the peak value of strain, Rp and ΔRp are, respectively, the projected range and the straggling of the distribution.

The H-platelets are modeled here as dislocation loops of interstitial nature with an equivalent Burgers vector \vec{b}_H ($\vec{b}_H = -b_H \vec{n}$ for interstitial loops, where \vec{n} is the unitary Burgers vector).^{3,17,18} Hence, the total formation energy E_f under the influence of an external stress is given by

$$E_f = E_{sf} + E_{\Sigma} = E_{sf} - \int \vec{b}_H \cdot \vec{\Sigma} \cdot d\vec{S}, \quad (4)$$

where E_{sf} is the self-formation energy of the precipitate, E_{Σ} is the energy term introduced by the external stress tensor $\vec{\Sigma}$, and $d\vec{S} = ds \cdot \vec{n}$ is a unit surface element of the platelet. With $b_H ds = dv$, from Eq. (4), we can write that the variation of energy by unit of volume introduced by an external stress is

$$\Delta E_{\Sigma} = \frac{dE_{\Sigma}}{dv} = \vec{n} \cdot \vec{\Sigma} \cdot \vec{n}. \quad (5)$$

The spatial distribution of the in-plane stress induced by the implantation is only depth dependent. The calculations are then presented in 2D considering the yz plane (where $y = [-1-10]$ and $z = [001]$ lattice directions), and Eq. (5) can be re-written as

$$\begin{aligned} \Delta E_{\Sigma} &= - \begin{pmatrix} n_z \\ n_y \end{pmatrix} \begin{pmatrix} \sigma_{zz} & \sigma_{zy} \\ \sigma_{yz} & \sigma_{yy} \end{pmatrix} \begin{pmatrix} n_z \\ n_y \end{pmatrix} \\ &= -(n_y^2 \sigma_{yy} + 2n_y n_z \sigma_{zy} + n_z^2 \sigma_{zz}), \end{aligned} \quad (6)$$

where n_y and n_z are the projected values of the \vec{n} on the y and the z -axes. According to the plane-stress approximation, Eq. (6) is simplified to

$$\Delta E_{\Sigma} = -n_y^2 \sigma_{yy}. \quad (7)$$

Three different orientations of the H-platelet, (111), (001), and (100), schematically presented in Fig. 2(a), were considered in the calculations. Their \vec{n} components in the yz plane are $\vec{n}_{(111)} = \left(-\sqrt{\frac{2}{3}}, \frac{1}{\sqrt{3}}\right)$, $\vec{n}_{(001)} = (0, 1)$, and $\vec{n}_{(100)} = (1, 0)$. For the (001)-platelets, Eq. (7) equals to zero. The variation of the formation energy induced by the in-plane stress is therefore null, and consequently $E_{f(001)} = E_{sf(001)}$. For the (111)-platelets,

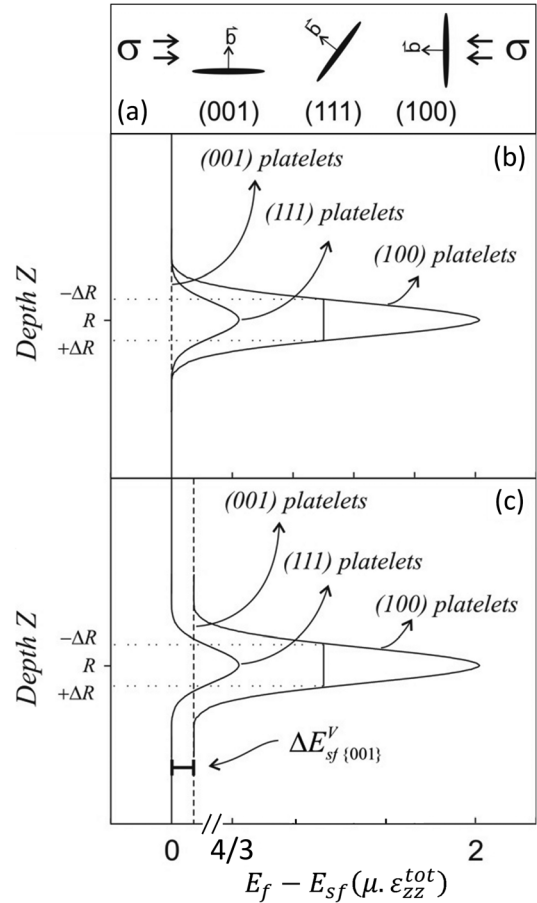


FIG. 2. (a) A schematic representation of the three considered orientations of H-platelets ((111), (001), and (100)), their equivalent Burgers vector, and the direction of the in-plane stress. Curves representing the variations along the depth z of the barrier of energy ascribed to the in-plane stress over the nucleation of (111), (001), and (100)-oriented H-platelets by considering (b) similar self-energies and (c) taking $\Delta E_{sf\{001\}}^V = E_{sf\{001\}}^V - E_{sf\{111\}}^V > 0$.

$$\Delta E_{\Sigma}^{(111)} = \frac{4}{3} \mu \epsilon_{zz}^{tot}, \quad (8)$$

and, for (010) or (100)-platelets

$$\Delta E_{\Sigma}^{(100)} = 2 \mu \epsilon_{zz}^{tot}. \quad (9)$$

Therefore, the in-plane stress imposes an energetic barrier for the nucleation of H-platelets along the {111} and (100) planes. The barrier, given by Eqs. (8) and (9), is approximately 65% higher for the (100)-orientation perpendicular to the surface, explaining the infrequent observation of this crystallographic variant.

The curves representing the barrier of energy as a function of depth in the substrate for the formation energy of the three considered orientations of platelet are plotted in Fig. 2(b) by considering similar self-formation energies¹⁹ for {111} and {001}-type orientations. According to this scenario, the nucleation of (001)-platelets would be preferentially observed all along the implanted layer. The observation of the predominant {111}-oriented H-platelets in the regions of lower in-plane stress suggests that the self-formation energy follows the relation

$$E_{sf(100)}^V > E_{sf(111)}^V. \quad (10)$$

The fact that only $\{111\}$ -oriented platelets are observed in the absence of external stresses, for example, when H is introduced in Si using plasma sources²⁰ also supports this hypothesis. Even if a difference in the self-formation energies favoring the $\{111\}$ -precipitates manifests from experimental observation, its magnitude is weak in comparison with the effect of stresses in the central region of the implanted layer. In Fig. 2(c), the barriers of energy for the three considered orientations platelets are represented considering the relation expressed in Eq. (10).

B. The effect of a local nanoscopic strain-field on the organization of H-platelets (experiment II)

In the second part of this work, the experiments and modeling of the effects of a mechanical stress in the arrangement of H-platelets were studied by introducing 3D nano-scale stress-fields in the system.

After the first fabrication step (45 keV He⁺ at the fluence of $1 \times 10^{16} \text{ cm}^{-2}$ followed by annealing at 350 °C for 900 s), the material was characterized to verify the formation of the stress sources embodied by the He-plates. The cross-section TEM micrograph in Fig. 3(a) shows two edge-on oriented He-plates lying on (001) planes running parallel to the surface. The depth location of $\approx 400 \text{ nm}$ corresponds roughly to the prediction given by SRIM code. A more detailed image of a single He-plate is shown in Fig. 3(b). The dark fringes surrounding the defect are ascribed to a diffraction contrast resulting from the distortion of the crystal lattice by the internal gas pressure of the cavity.⁴ The plan-view in Fig. 3(c) shows the circular nature of the object evidencing its cylindrical symmetry around a virtual axis z .

After characterization of the He-plates, the substrate was submitted to the second step of fabrication (30 keV H₂⁺ at the fluence of $0.5 \times 10^{16} \text{ cm}^{-2}$ followed by 300 °C for 1800 s) to create the H-platelets under the influence of the local stress-fields. A TEM micrograph of the implanted/annealed system is displayed in Fig. 4. It shows that, above the He-plate, H-platelets are preferentially aligned to $\{111\}$ crystallographic directions with respect to the vertical symmetry axis z of the stress-field. Two edge-on $\{111\}$ variants are observed when imaging along the $[-110]$ direction of the crystal. The complementary variants would be seen by imaging along the perpendicular direction $[-1-10]$. The pictographic representation in the bottom of Fig. 4 summarizes the scenario; local strain fields from individual He-plates inducing specific arrangements of H-platelets creating nanoscopic ordered domains. Elsewhere, far from range from the local field, the configuration of H-platelets is similar to the one in Fig. 1(b).

In Fig. 5, we display a TEM image captured from a thinner region of the specimen. There, the observed He-plate was sectioned, resulting in a non-pressurized cavity: the strain-contrast is not observed. This image shows in detail the distribution of two $\{111\}$ variants of H-platelets. On its top, the frequency count of platelets versus the distance from the central z -axis is plotted.

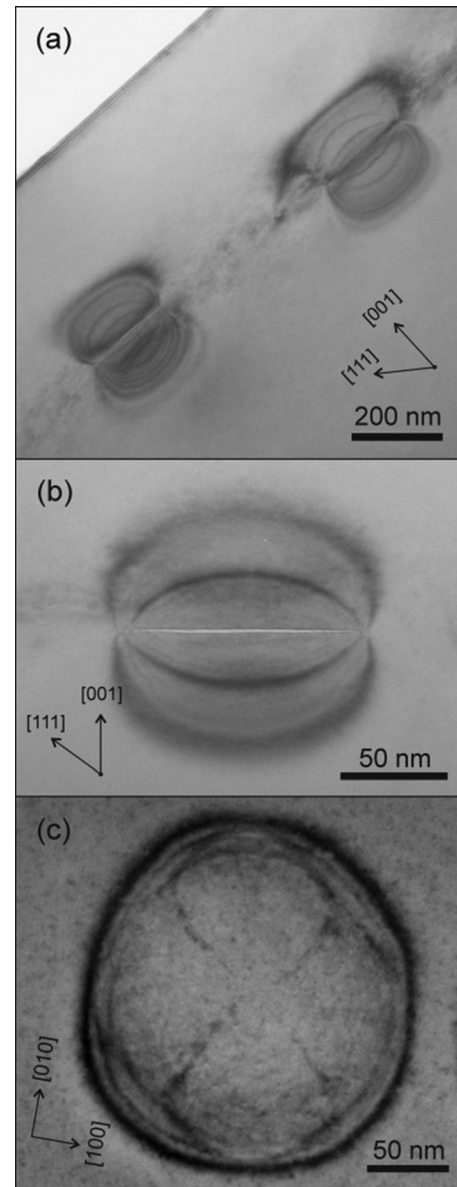


FIG. 3. (a) Cross-sectional TEM micrograph showing two edge-on He-plates fabricated by implanting 45 keV He⁺ at $1 \times 10^{16} \text{ cm}^{-2}$ and annealing at 350 °C for 900 s. (b) A detailed imaging of a single He-plate. (c) A plan-view micrograph of a He-plate defining the circular character of the object. The image was obtained using multiple g vectors exposing a fourfold contrast ascribed to bend contours.

To develop a model allowing to describe these observations, the following hypotheses were made: (i) the preferential orientation for the nucleation of H-platelets is determined by the minimization of their formation energy with respect to the external stress tensor,^{3,11} and (ii) the system is located close to a free surface and this must be accounted to calculate the distribution of stresses, by considering a semi-infinite solid. As in Sec. I, H-precipitates were modeled as extrinsic type dislocation loops. The variation of the energy of formation under the influence of a stress-field is given by Eq. (5). However, the stress tensor Σ has two contributions now: (i) the local stress-field introduced by the He-plates and (ii) the in-plane stress generated by the H implantation.

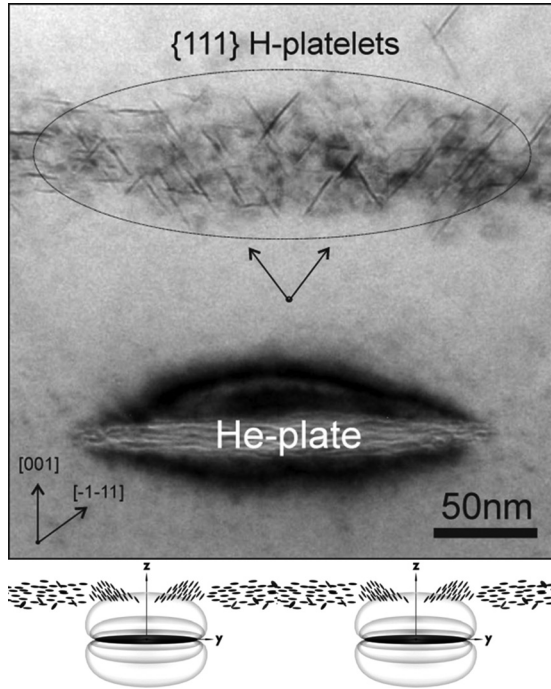


FIG. 4. Cross-sectional TEM micrograph obtained after the two steps of implantation/annealing (45 keV He^+ at $1 \times 10^{16} \text{ cm}^{-2}$ and annealing at 350°C for 900 s + 30 keV H_2^+ at $0.5 \times 10^{16} \text{ cm}^{-2}$ and annealing at 300°C for 1800 s) showing the He-plate and the particular distribution of H-platelets oriented by the local stress field. At the bottom is a pictographic representation of the system: {111}-platelets arrangements under the influence of He-plates and (001)-platelets preferentially formed far from the local strain sources. The distance between nano-arranged domains usually exceeds their average diameter.

The strain-field of a He-plate must now be calculated. For this, we modeled the structure as an extrinsic type dislocation loop with an effective Burgers vector ($b_{\text{eff}}^{\text{He-plate}}$) to account for the displacement-field introduced by the internal gas pressure. A 2D cut of the dislocation loop over its center

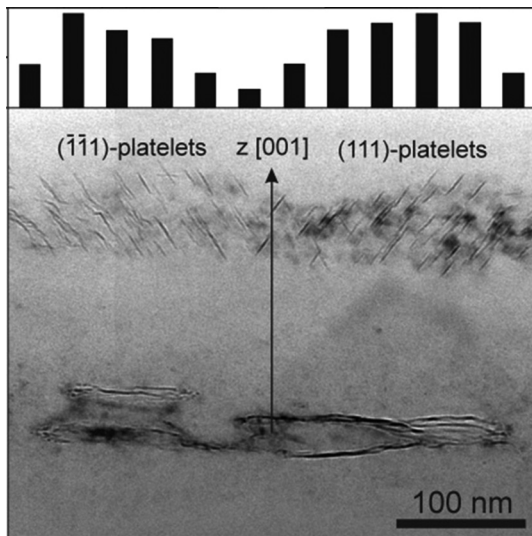


FIG. 5. Cross-sectional TEM micrograph obtained from a thin region of the specimen where the He-plates were sectioned by the foil surfaces. A detailed view of the distribution of two edges-on variants of H-platelets ($\bar{1}\bar{1}1$ at the left and 111 at the right) is observed. At the top is a frequency count histogram of H-platelets as a function of the distance from the axis z represented in the figure.

can be represented by a dipole of edge dislocations. The components of the stress field in a semi-infinite solid are obtained by solving the appropriate Airy stress function¹⁸ φ such that $\sigma_{zz} = \frac{\partial^2 \varphi}{\partial y^2}$, $\sigma_{yy} = \frac{\partial^2 \varphi}{\partial z^2}$, and $\sigma_{zy} = -\frac{\partial^2 \varphi}{\partial z \partial y}$. For an edge dislocation of Burgers vector $(0, b)$ in an infinite elastic medium, it is a typical/standard problem, and the solution is given by¹⁸

$$\varphi(z, y) = -D \ln \sqrt{z^2 + y^2}, \quad (11)$$

where $D = \frac{\mu b_{\text{eff}}}{2\pi(1-\nu)}$, μ the shear modulus, and ν the Poisson's ratio of the material.

To consider the proximity of a free surface on the distribution of stresses, a restrict condition has to be satisfied: the normal and shear stresses on the surface (defined as $z=0$) vanish, or

$$\sigma_{zz}(y, 0) = 0, \quad (12)$$

and

$$\sigma_{zy}(y, 0) = 0. \quad (13)$$

To satisfy Eq. (12), a virtual image dislocation with opposed Burgers vector $(0, -b)$ is introduced at the image point. To equilibrate the tangential forces (Eq. (13)), we introduced Boussinesq forces on the surface.¹⁸ The Airy's function for our system can be written then as

$$\varphi(y, z) = \varphi^{\text{edge}}(y, z) + \varphi^{\text{image}}(y, z) + \varphi^{\text{Boussinesq}}(y, z). \quad (14)$$

For a dipole of edge dislocation running along the y -axis, separated by a length $2a$, at a distance $-c$ from the surface and centered in the z -axis (with $|c| = 4|a|$) it follows that

$$\begin{aligned} \varphi^{\text{dipole}}(y, z) = & -Dy \ln \sqrt{(z+c)^2 + (y+a)^2} \\ & + Dy \ln \sqrt{(z-c)^2 + (y+a)^2} + \frac{2Dazy}{(z-c)^2 + y^2} \\ & + Dy \ln \sqrt{(z+c)^2 + (y-a)^2} \\ & - Dy \ln \left(\sqrt{(z-c)^2 + (y-a)^2} \right) \\ & - \frac{2Dazy}{(z+c)^2 + y^2}. \end{aligned} \quad (15)$$

We have normalized the function by a/D and added the in-plane stress component in the tensor, giving

$$\varphi^{\text{norm}}(y, z) = \frac{a}{D} \varphi^{\text{dipole}}(y, z) + \frac{a}{D} \sigma_{\parallel} \frac{y^2}{2}. \quad (16)$$

The total stress components are finally calculated in terms of the reduced quantities

$$\begin{aligned} \sigma_{zz}^*(y, z) &= \frac{\partial^2 \varphi^{\text{norm}}(y, z)}{\partial y^2}, \quad \sigma_{zy}^*(y, z) = -\frac{\partial^2 \varphi^{\text{norm}}(y, z)}{\partial z \partial y} \quad \text{and} \\ \sigma_{yy}^*(y, z) &= \frac{\partial^2 \varphi^{\text{norm}}(y, z)}{\partial z^2}. \end{aligned} \quad (17)$$

The last step is to calculate the value of $b_{eff}^{He-plate}$. For this, we combined the calculations of $\sigma_{zz}^{*0}(0, -c)$ with the equation of equilibrium pressure of a gas-filled plate^{21,22} thus obtaining

$$b_{eff}^{He-plate} = \sqrt{\frac{\pi\gamma\mu}{r(1-\nu)} \frac{2\pi r(1-\nu)}{\mu\sigma_{zz}^{*0}}}, \quad (18)$$

where γ is the specific surface free energy and $r=100$ nm is a typical value for the radius of a He-plate. The result from the calculations of σ_{zz} along the central axis of the dipole (i.e., for $y=0$) allows to obtain that $\sigma_{zz}^{*0}(0, -c)=1.8$. Taking for Si that $\gamma=1.38$ Jm⁻², $\mu=68$ GPa, and $\nu=0.22$, we obtain that $b_{eff}^{He-plate} \approx 7$ nm. This value is obtained considering all the hypothesis and approximations of the 2D model, representing therefore an estimated order of magnitude. The in-plane stress induced by H implantation was calculated from Eq. (2) for the maximum value of strain $\epsilon_{zz}^{MAX} \approx 0.35\%$. This approach was chosen because it allows representing in a single map the energy variation for H-platelets to different implantation depths.

For the experimentally observed platelets of (001) and (111) orientation, the maps of the variation of energy ΔE introduced by the combined effects of in-plane stress and stress field from a dipole of dislocations are displayed in Figs. 6(a) and 6(b). The iso-regions in the figure are plotted in intervals of 0.1, which corresponds to ≈ 100 MPa. The unit length $a=100$ nm. The depth location of H-implantation is indicated by the horizontal dotted lines in Figs. 6(a) and 6(b). The plot for the (001)-platelets displays

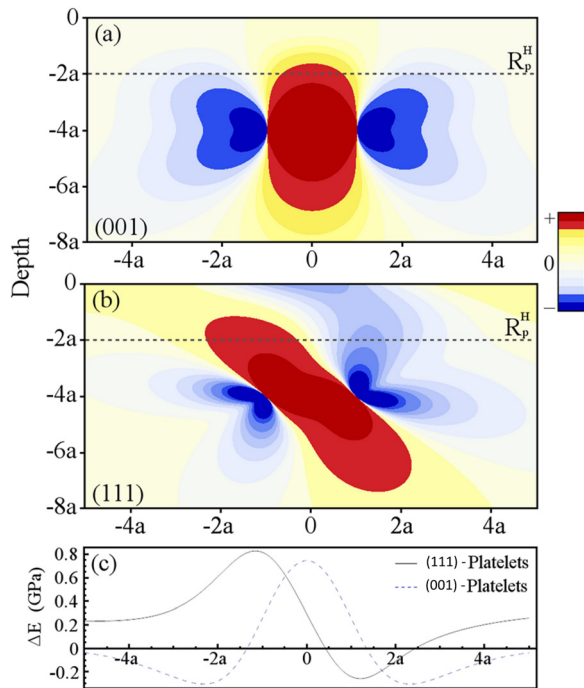


FIG. 6. Contour maps of the energy variation for the formation of (a) (111) and (001)-platelets under the influence of the cylindrical stress field generated by the He-plate located at the depth of $-4a$ and extending from $-a$ to a along the horizontal axis. The surface of the wafer sits at depth $z=0$. A level curve at the depth of $-2a$, corresponding to the depth of implantation in the experiments is shown in (c) for the (001) (full line) and (111)-platelets (dotted line).

the symmetrical character around the central vertical axis of the stress field emerging from the dislocation dipole. The map for the variation of energy of (111)-platelets, on the other hand, shows a significant asymmetry where each of the {111} variants will be privileged in a respective quadrant of the volumetric 3D structure. Figure 6(c) is a level curve from the map in Figs. 6(a) and 6(b). It represents the variation of energy at the depth $z=200$ nm, where the H-platelets were created. At the right side from the symmetry axis z , the formation of (111)-platelets is strongly favorable from $y=0$ to $y \approx 1.5a$. From $y \approx 1.5a$, the (001) orientation becomes preferential. On the left side of the curve, the (111)-platelets have a high barrier for nucleation explaining why another {111} variant appears. The examination of the frequency count in Fig. 5 also evidences a clear relationship to the energy variation curves for the {111} platelets in Figs. 6(b) and 6(c). Hence, the proposed model helps to explain not only the spatial position for the preferential formation of the crystallographic variants but also it seems to provide a good description of the corresponding relative densities as a function of the distance from the stress source as well.

C. Prediction of the model

The extrapolation of the proposed model reveals interesting features. Figure 7 shows the energy variation curves calculated considering different H-implantation depths z . The He-plate depth position is at $z=-400$ nm, i.e., the curves from -50 nm to -350 nm refer to H implantation depths above the He-plate. The region where the (111)-platelets are favorable is approximately centered at $y \approx 100$ nm and becomes narrower as it approaches the strain source. For $z=-350$ nm, this variant is quite unlikely to be formed. The formation of (100)-platelets may be favorable, but we have not observed, at a very narrow region located along the z -axis. For $z < -400$ nm underneath the He-plate, close to the strain source the general feature of the curves is basically the same to those shown for $z > -400$ nm. The (111) curve is inverted, as expected, and therefore this variant is favorable in the opposite side of the structure. The free-surface effect in the stress distribution, and consequently in the calculated energy variations, is evident considering a certain absolute distance z from the He-plate. Let us compare, for example, the curves obtained for ± 350 nm from the strain source (i.e., the curve for $z=-50$ nm with $z=-750$ nm). For a larger distance from the He-plate, the curve for $z=-1000$ nm shows that the effect of the local strain source becomes negligible, and the orientation of H-platelets is determined by the in-plane stress uniquely, being the (001)-variant parallel to the surface the preferential one.

The model can be also used to predict the orientations when the intensity of the in-plane stress varies, for example, by changing the H-implantation fluence^{8,9} or the character of the stress by introducing tensile layers in the substrate.²³ Figure 8 shows the energy variation maps predicted by changing the environment of nucleation for H-platelets from a highly tensile layer ($k=-2$) to a highly compressive layer ($k=2$), with the factor k being the second term of Eq. (16). Obviously, (001)-platelets are neither affected by the

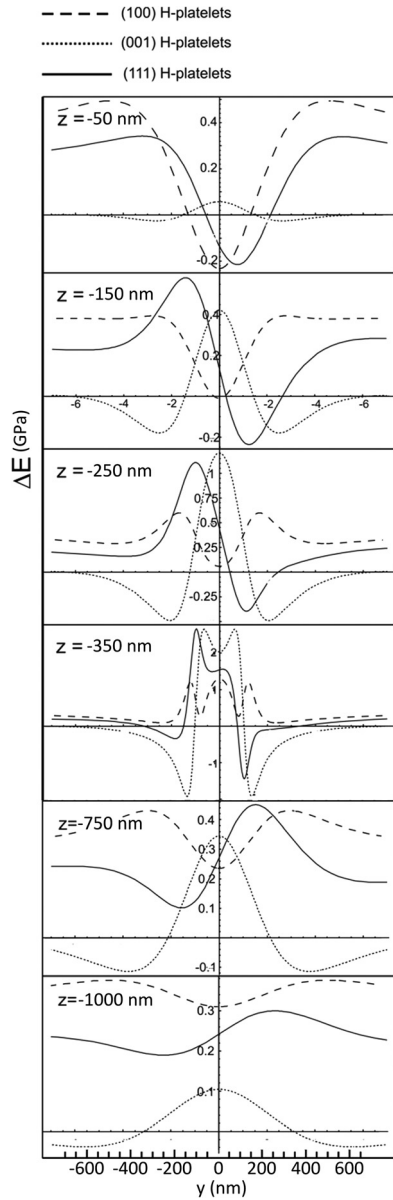


FIG. 7. Level curves of the variation of energy introduced by the elastic stress tensor (ΔE) for (001), (100), and (111)-platelets orientation from the depth $z = -50$ nm to $z = -350$ nm, at the upper side of the He-plate (localized at $z = -400$ nm from $y = -100$ nm to $y = +100$ nm) and at the lower side for the depths $z = -750$ nm and $z = -1000$ nm.

changes of intensity nor the in-plane stress sign. On the other hand, (100)-platelets perpendicular to the surface become strongly favorable under tensile in-plane stress conditions, in accordance with observations,¹⁶ and unfavorable in

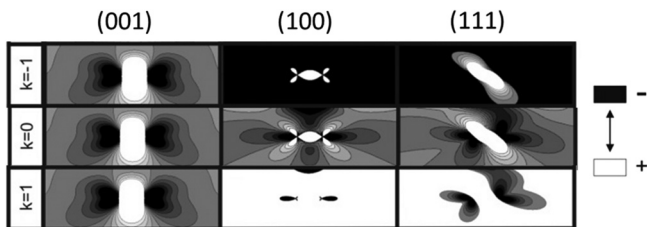


FIG. 8. Energy variation maps for (001), (100), and (111)-oriented H-platelets. The maps show the evolution of the distributions for different values of k , related to the intensity and character (compressive or tensile) of the in-plane stress.

compressive stress conditions. In general, (111) platelets also become more favorable under tensile stress conditions than in compressive one.

D. 3D model

To calculate the stress fields and solve Eq. (5) for the variation of energy in 3D, we have developed a full anisotropic model of the structure using finite element method (FEM), implemented in the commercial code COMSOL. To model the stress field from the He-plate, we introduced an oblate spheroid cavity with the semi-principal axis $a = b = 100$ nm and $c = 1.5$ nm, at 400 nm depth from the free surface of a (001) Si matrix. The in-plane stress was introduced as a constant value of $\sigma_{||} = -2\mu\epsilon_{zz}^{MAX} = -0.483$ GPa. The elastic constants for the Si matrix were $C_{11} = 165.7$ GPa, $C_{12} = 63.9$ GPa, and $C_{44} = 79.6$ GPa. The volume considered in the calculations is twice the diameter of the cavity and $1.2 \mu\text{m}$ of total vertical length. The lateral boundaries were set with periodic conditions simulating the presence of neighboring cavities, and for reference, the bottom was fixed to zero vertical displacement. A pressure normal to the internal surfaces of the cavity was the calculated value of 1.8 GPa (see Sec. III B).

In Fig. 9(a), we display a 3D plot of iso-values contour map showing the variation of energy for the (111)-platelets nucleation around the pressurized He-plate. The regions of blue contrast refer to negative values, favoring the nucleation. Red areas are of positive energy variations increasing the barrier for nucleation of (111)-platelets. Figs. 9(b) and 9(c) are vertical slices of planes zy at two positions along the x -axis: (i) $x = 0$ at the centre of the structure and (ii) $x = 200$ nm corresponding to the border of the crack. Figure 9(b) would basically be the analogue of Fig. 6(b), calculated for 2D using the analytical model. Figure 9(c) shows that the regions of positive values reduce considerably at the border of the crack and the negative areas predominate.

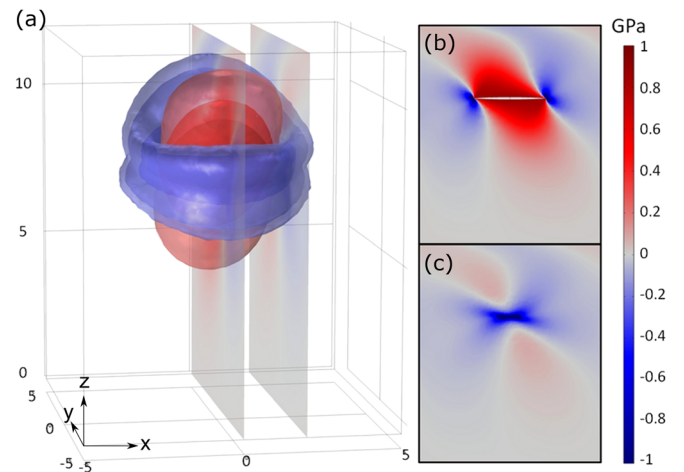


FIG. 9. (a) 3D iso-contour maps of the energy variation for the formation of (111)-oriented H-platelets under the influence of the cylindrical stress field generated by the He-plate. The position of vertical slice cuts plotted in (b) for the center of the structure and (c) for the radius of the crack is depicted in (a).

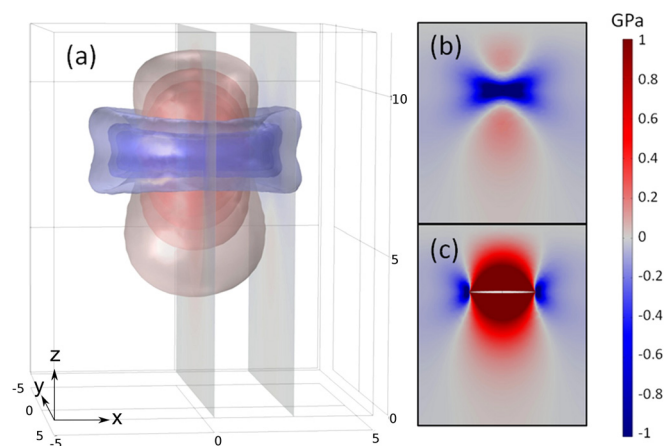


FIG. 10. (a) 3D iso-contour maps of the energy variation for the formation of (001)-oriented H-platelets under the influence of the cylindrical stress field generated by the He-plate. The position of vertical slice cuts plotted in (b) and (c) is depicted in (a).

The 3D contour maps in Fig. 10(a) show the cylindrical symmetry of the distribution for the (001)-variant. Vertical slice cuts showing the evolution of energy distribution from the central to the border region of the strain source are displayed in Figs. 10(b) and 10(c). While positive values predominate in the middle, negative regions are mostly found at the border.

IV. CONCLUSIONS

Using H and He implantation in Si, a concept for the organization of precipitates using local strain-engineering was presented and discussed. In the first part of the work, we studied and modeled the effect of the global scale stress introduced by the lattice damage on the formation of H-platelets. In general, there is a tendency to find the crystallographic variant which is parallel to the surface, in the present case the (001)-platelets. The experimental observations of {111}-oriented platelets at the edges of the implanted layer led to the speculation that the self-formation energy of {111}-platelets is lower than that of {001}-platelets. In the second part of the work, the effect of a local stress on the nucleation of H-platelets was studied by introducing localized stress field sources of nanometer scale. The observations demonstrate that the nanoscopic strain fields of cylindrical character determined the organization of H-platelets in a fourfold distribution, and discrete arranged domains within a solid matrix were then created. We developed analytical 2D and numerical 3D models of the system based on elastic interactions to modulate the formation energy of different crystallographic variants of platelets. The obtained results are in good agreement with the experimental observations.

The concept of using embedded local strain fields to manipulate precipitates has the potential to: (i) be further developed to create specific arrangements according to the characteristics of the strain source, and (ii) favor the formation of crystallographic variants that are, in principle, unlikely to be formed due to a higher self-energy, as it is the case of (001) platelets in Si, which appears only due to a favorable stress configuration in the surrounding matrix.

ACKNOWLEDGMENTS

The authors gratefully acknowledge CAPES COFECUB program, CNPq, Ecole doctorale SP@MA, PETROBRAS S. A., Laboratório de Implantação Iônica (UFRGS), and Centro de Microscopia Eletrônica (UFRGS).

- ¹W. Lu and C. M. Lieber, *Nature Mater.* **6**, 841–850 (2007).
- ²D. Mijatovic, J. C. T. Eijkel, and A. van den Berg, *Lab Chip* **5**, 492–500 (2005).
- ³S. Reboh, M. F. Beaufort, J. F. Barbot, J. Grilhé, and P. F. P. Fichtner, *Appl. Phys. Lett.* **93**, 022106 (2008).
- ⁴P. F. P. Fichtner, J. R. Kaschny, R. A. Yankov, A. Mucklich, U. Kreibitz, and W. Skorupa, *Appl. Phys. Lett.* **70**, 732 (1997).
- ⁵N. Hueging, M. Luysberg, K. Urban, D. Buca, and S. Mantl, *Appl. Phys. Lett.* **86**, 042112 (2005).
- ⁶N. Hueging, M. Luysberg, H. Trinkaus, K. Tillmann, and K. Urban, *J. Mater. Sci.* **41**, 4454–4465 (2006).
- ⁷S. Reboh, J. F. Barbot, M. F. Beaufort, and P. F. P. Fichtner, *Appl. Phys. Lett.* **96**, 031907 (2010).
- ⁸N. Sousbie, L. Capello, J. Eymery, F. Rieutord, and C. Lagahe, *J. Appl. Phys.* **99**, 103509 (2006).
- ⁹C. Miclaus and M. S. Goorsky, *J. Phys. D: Appl. Phys.* **36**, A177 (2003).
- ¹⁰S. Reboh, F. Schaurich, A. Declémy, J. F. Barbot, M. F. Beaufort, N. Cherkashin, and P. F. P. Fichtner, *J. Appl. Phys.* **108**, 023502 (2010).
- ¹¹M. Nastasi, T. Höchbauer, J.-K. Lee, A. Misra, J. P. Hirth, M. Ridgway, and T. Lafford, *Appl. Phys. Lett.* **86**, 154102 (2005).
- ¹²J. F. Ziegler, J. P. Biersack, and U. Littmark, *The Stopping and Range of Ions in Solids* (Pergamon Press, New York, 1985).
- ¹³S. A. Stepanov, See <http://sergey.gmca.aps.anl.gov/> for details on the simulation of XRD and access to the simulation server.
- ¹⁴F. Rieutord, F. Mazen, S. Reboh, J. D. Penot, L. Bileanu, J. P. Crocombette, V. Vales, V. Holy, and L. Capello, *J. Appl. Phys.* **113**, 153511 (2013).
- ¹⁵A. Debelle and A. Declémy, *Nucl. Instrum. Methods Phys. Res. B* **268**, 1460–1465 (2010).
- ¹⁶A. Debelle, A. Boule, F. Rakotovo, J. Moeyaert, C. Bachelet, F. Garrido, and L. Thomé, *J. Phys. D* **46**, 045309 (2013).
- ¹⁷J. H. Neethling and H. C. Snyman, *J. Appl. Phys.* **60**, 941 (1986).
- ¹⁸J. P. Hirth and J. Lothe, *Theory of Dislocations* (Wiley, New York, 1982).
- ¹⁹N. Martsinovich, I. S. Martínez, and M. I. Heggge, *Phys. Status Solidi C* **2**, 1771 (2005).
- ²⁰N. H. Nickel, G. B. Anderson, N. M. Johnson, and J. Walker, *Phys. Rev. B* **62**, 8012 (2000).
- ²¹M. Hartmann and H. Trinkaus, *Phys. Rev. Lett.* **88**, 055505 (2002).
- ²²S. Reboh, A. A. de Mattos, J. F. Barbot, A. Declémy, M. F. Beaufort, R. M. Papaléo, C. P. Bergmann, and P. F. P. Fichtner, *J. Appl. Phys.* **105**, 093528 (2009).
- ²³A. J. Pitera and E. A. Fitzgerald, *J. Appl. Phys.* **97**, 104511 (2005).